The Astrophysical Journal, 730:114 (8pp), 2011 April 1 doi:10.1088/0004-637X/730/2/114
© 2011. The American Astronomical Society. All rights reserved. Printed in the U.S.A.

THE DISSIPATION OF SOLAR WIND TURBULENT FLUCTUATIONS AT ELECTRON SCALES

Enrico Camporeale[1] and David Burgess
School of Mathematical Sciences, Queen Mary University of London, Mile End Road, London E1 4NS, UK
Received 2010 August 10; accepted 2011 January 25; published 2011 March 10

ABSTRACT

We present two-dimensional fully kinetic particle-in-cell simulations of decaying electromagnetic fluctuations. The computational box is such that wavelengths ranging from electron to ion gyroradii are resolved. The parameters used are realistic for the solar wind, and the ion-to-electron mass ratio is physical. The dissipation of turbulent fluctuations at small scales is thought to be a crucial mechanism for solar wind acceleration and coronal heating. The computational results suggest that a power-law cascade of magnetic fluctuations could be sustained up to scales of the electron Larmor radius and smaller. We analyze the simulation results in light of the Vlasov linear theory, and we comment on the particle heating. The dispersion curves of lightly damped modes in this regime suggest that a linear mechanism could be responsible for the observed steepening of power spectra at electron scales, but a straightforward identification of turbulent fluctuations as an ensemble of linear modes is not possible.

Key words: plasmas – solar wind – turbulence – waves

Online-only material: color figures

1. INTRODUCTION

The solar wind is a collisionless medium which is known to be turbulent over many length and timescales. The first observations of an active turbulent cascade at large scales in the solar wind date back to the work of Coleman (1968). Analogous to hydrodynamic turbulence, the large-scale fluctuations are expected to nonlinearly cascade to smaller scales and be ultimately dissipated in the so-called dissipation range. However, in a collisionless plasma, ordinary viscosity cannot play a decisive role for the dissipation of energy, as it does in a neutral fluid. Hence, it has been long thought that the onset of the dissipation range in the solar wind must be associated with cyclotron or Landau damping, and therefore must lie within kinetic scales.

The understanding of the mechanisms that convert the electromagnetic turbulent energy into kinetic heating is far from complete. This issue is very relevant for the development of a realistic scenario of solar wind acceleration and coronal heating.

The non-hydrodynamic nature of the physics involved in the dissipation process is now widely appreciated (Smith et al. 2006), and the understanding of dissipation mechanisms at small scales represents a very active field of research.

Observations indicate that kinetic plasma physics at both proton and electron scales are involved (Matthaeus et al. 2008). Moreover, it is known that the Kolmogorov-like inertial range power spectrum terminates at ∼0.3 Hz, where the spectrum of magnetic fluctuations steepens to form a power law with an average index close to −3 and varying between −2 and −5. (Leamon et al. 1998a, 1998b, 1999). More recent observations (Sahraoui et al. 2009, 2010) have shown that the power law in the range of scales between ion and electron gyroradii is quite universal and close to 2.8. They also suggested the possibility that a nonlinear turbulent cascade could proceed further above the frequency associated with electron gyromotion, where the power spectrum supposedly undergoes another abrupt break and steepening. This interpretation has been challenged by observations reported in Alexandrova et al. (2009) that suggest an exponential roll over of the power spectrum at electron scales, which is usually interpreted as the onset of linear dissipative mechanisms.

In the last few years, an intensive effort has been directed to understand the mechanism that regulates the damping of turbulent fluctuations at small scales through a number of different approaches involving numerical simulations. In particular, Howes et al. (2008b) have performed state-of-the-art gyrokinetic simulations of kinetic Alfvèn waves (KAWs) cascade; particle-in-cell (PIC) simulations of decaying whistler modes have been performed by Saito et al. (2008); and Svidzinski et al. (2009) have presented PIC simulations of fast magnetosonic waves. Hybrid simulations have been presented by Parashar et al. (2009) and Markovskii et al. (2010), and a shell model for three-dimensional Hall-MHD has been studied by Galtier & Buchlin (2007).

Interestingly, many works in this area have made the assumption that there must be a certain length scale where the amplitude of magnetic fluctuations becomes so small that it is justifiable to treat the turbulent dissipation as the damping of linear waves. Therefore, the spectrum of magnetic fluctuations has been tentatively compared to linear theory predictions in a number of papers (Li et al. 2001; Stawicki et al. 2001; Howes et al. 2008a; Gary et al. 2008; Jiang et al. 2009; Podesta et al. 2010). Here, it is (sometimes implicitly) assumed that linear damping mechanisms can convert electromagnetic energy to kinetic energy with the same efficiency and rate in a turbulent system and in a homogeneous plasma in thermodynamical equilibrium. This approach has been recently challenged in Camporeale et al. (2010), where it is argued that using the least damped modes of a normal mode linear analysis might be a misleading way to characterize the dissipation.

In any case, if any linear mode is dominant in regulating the cascade in the dissipation range, there is certainly no agreement on which mode that should be (Gary & Smith 2009). It has to be mentioned that the numerical approach mentioned above and pursued by many researchers has so far focused on ion scales, not extending very deeply into electron scales, mainly for reasons of computational costs.

[1] Now at the Applied Mathematics and Plasma Physics Group, Theoretical Division, Los Alamos National Laboratory, Los Alamos, NM 87545, USA.

The aim of this paper is to present fully kinetic PIC simulations of decaying electromagnetic fluctuations at electron scales. In doing so, we address the following open problems. It is still unknown whether a linear approximation for the damping rate of the fluctuations, that would effectively describe the waves as an ensemble of linear modes, is fully justifiable and at which scale that approximation becomes valid. Moreover, there is an open debate about the scale at which such fluctuations are expected to be completely dissipated, and what mechanism is responsible for the dissipation. As we will show, our results do not support a scenario where turbulent fluctuations can be described as an ensemble of the least damped linear waves, not even at very small scales, although the observed steepening of the power spectra might be associated with the steepening of the dispersion curves of linear modes.

The feasibility of the simulations presented in this paper has been greatly enhanced by using a semi-implicit method both for the field solver and the particle mover, and we will discuss some computational issues that have emerged in this study and that should be taken into account for future studies.

The paper is organized as follows. Section 2 briefly describes the PIC code, the parameters used, the issues related to the initialization of the simulations, and compares this paper with previous works. The main results are described in Section 3. The emphasis will be on the observed nonlinear cascade, the identification of linear modes, and particle heating. The conclusions and discussion of future work are given in Section 4.

2. METHODOLOGY

We perform simulations of an ion–electron plasma in a two-dimensional periodic box in Cartesian geometry (x, y). The code used is a fully kinetic, electromagnetic, parallel PIC code, called *PARSEK2D*. The main feature of the code is the use of an implicit moment method for advancing the fields in time and a predictor–corrector routine to advance the particles. A thorough description of the algorithm and the code can be found in Markidis et al. (2009). The implicitness of the scheme allows a relaxation of the stability conditions typical of an explicit code. In particular, the cell size Δx is not required to be comparable with the Debye length, the time step Δt can be larger than the inverse plasma frequency and, in general, the factor $c\Delta t/\Delta x$ (where c is the speed of light) can be larger than 1.

For the simulations presented in this paper, we have found that it is still convenient, for accuracy reasons, to resolve the inverse electron plasma frequency. The cell size Δx, however, is about 20 times the Debye length, and the Courant factor $c\Delta t/\Delta x$ is about 9. Therefore, the total saving with respect to an explicit code is at least a factor of 80,000 (not taking into account the complexity of the algorithm). This large saving factor translates into the possibility of simulating a plasma in realistic conditions in a computational box that is fairly large. We compare in Figure 1 the range of wavevectors included in the computational box for the simulations presented in this paper with previous works. Table 1 compares other relevant parameters, such as the ratio of plasma to cyclotron frequency (this is undefined in hybrid simulations) and the ion-to-electron mass ratio. Note that the use of an artificial mass ratio makes the values of the ion and electron gyroradii closer to each other, resulting in an extension of the range of wavevectors studied. This of course results in a computational advantage, but it is often difficult to estimate the effects of this approximation on the results, since it is very well known that the separation of ion and electron scales is an intrinsic and important characteristic of plasmas. What emerges

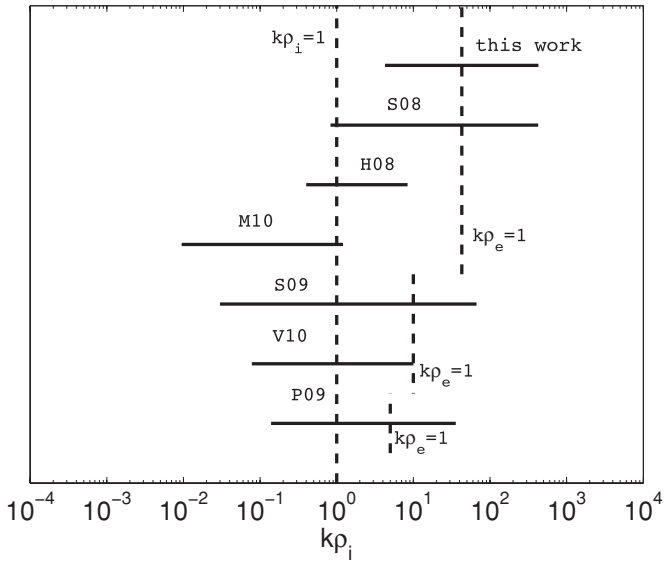

Figure 1. Comparison of the range of wavevectors studied in different works. The acronym list is reported in Table 1. The vertical dashed lines indicate the inverse proton Larmor radius ($k\rho_i = 1$), and the inverse electron Larmor radius ($k\rho_e = 1$), assuming equal ion and electron temperatures. Note that the latter is shifted in works that do not use a physical mass ratio. Also, note that V10 has reported simulations with different temperature ratios (and therefore different locations of $k\rho_e = 1$).

from Figure 1 is that, as far as we know, this paper presents the first simulations that use realistic parameters in a fairly large computational domain that extends to electron scales. We point out that also the work by Saito et al. (2008) was in principle able to extend to electron scales, but the number of particles used was too low to distinguish the results above $k\rho_i \sim 10$ from the noise level.

In this work, the plasma is in solar wind conditions. The electron plasma beta is equal to 0.5 ($\beta_e = 8\pi n_0 T_e/B_0^2$, where T_e is the electron temperature, n_0 is the density, and B_0 is the magnetic field intensity). Ions and electrons have initially equal temperatures and a Maxwellian distribution function. The ratio of ion plasma frequency to ion gyrofrequency ω_{pi}/Ω_i is about 1650, and the ion-to-electron mass ratio is physical ($m_i/m_e = 1836$). The number of cells is 200×200, and the box size is large enough to accommodate waves with wavenumbers k ranging from $k\rho_i = 4.28$ (equivalent to $k\rho_e = 0.1$) to $k\rho_e = 10$, where ρ_i and ρ_e are the ion and electron gyroradii, respectively. In all the simulations presented in this paper, we have used 6400 particles per cell, for each species, and the simulations are typically run for a time $T = 100\ \Omega_e^{-1}$ (Ω_e is the electron gyrofrequency).

The choice of initial conditions offers a wide degree of freedom. The general idea is to initialize a spectrum of fluctuations with properties somehow similar to the one observed in the solar wind and follow their decay in time. Some authors have performed simulations where a spectrum of only one plasma linear mode was excited at small values of k (for instance, KAWs, or whistlers). In order to do so, one should compute the phase and amplitude relations between different quantities such as magnetic and electric fields, velocity and density perturbation predicted by linear theory for any single value of k, and impose such perturbations to the background equilibrium. In order to get a completely self-consistent initial perturbation, the particle distribution function should be perturbed exactly. This is very expensive, from a computational point of view, and a shortcut

Table 1
Comparison of Different Parameters with Previous Works

Acronym	Reference	$k\rho_i$	ω_i/Ω_i	m_i/m_e	N_p	Type
···	This work	4.28–428.48	1650	1836	6400	2D-3V PIC
S08	Saito et al. (2008)	0.83–425	96	1836	64	2D-3V PIC
H08	Howes et al. (2008b)	0.4–8.4	···	1836	···	3D-2V Gyrokinetic
M10	Markovskii et al. (2010)	0.0095–1.21	192.3	···	1000	2D Hybrid
S09	Svidzinski et al. (2009)	0.03–66.7	15	100	>100	2D-3V PIC
V10	Valentini et al. (2010)	0.078–10.003	···	100	···	2D-3V Hybrid–Vlasov
P09	Parashar et al. (2009)	0.139–35.7	···	25	100	2D Hybrid

Notes. ρ_i is the ion gyroradius, ω_i/Ω_i is the ratio of ion plasma to cyclotron frequency (a typical value for the solar wind at 1 AU is around 4000), m_i/m_e is the ratio of ion to electron mass, and N_p is the number of particles per cell.

which is very often employed is to initialize the particles with a shifted Maxwellian distribution, such that only the current and charge densities are consistent with the linear theory predictions, but not all the higher-order moments of the distribution function. The implicit assumption of such a method is that the PIC code will be able to quickly "self-adjust" the initial inconsistency, but this approach remains, in our view, not very satisfactory. Moreover, the choice of the slope of the initial power spectrum constitutes yet another degree of freedom in the initialization.

In this work, we have opted for a very general initial perturbation. In this way, we do not face the problem of choosing some particular modes to initialize, and we are also able to study which mode, if any, "survives" through the nonlinear cascade. Accordingly, we initialize our simulations with a background magnetic field in the x-direction, and we superimpose a spectrum of random phase fluctuations in the magnetic field only. We assume that such a perturbation is general enough to perturb a large variety of waves in the plasma. We point out that, differing from the normal mode initialization described above, this choice is self-consistent both with the Vlasov and Maxwell equations. The plasma will certainly respond instantaneously to magnetic field gradients by creating currents and generating electric fluctuations, and ultimately waves. The only requisite that the initial perturbation must satisfy is to be divergence-free. Hence, we initialize the magnetic perturbations as

$$\delta B_x = \sum_{k_x}\sum_{k_y} |k_x|^{-(\alpha+1)}|k_y|^{-\beta}\cos(k_x x + k_y y + \phi_{x,y}) + \sum_{k_y}\left|\frac{2\pi}{L_x}\right|^{-(\alpha+1)}|k_y|^{-\beta}\cos(k_y y + \phi_x) \quad (1)$$

$$\delta B_y = -\sum_{k_x}\sum_{k_y} |k_x|^{-\alpha}|k_y|^{-(\beta+1)}\cos(k_x x + k_y y + \phi_{x,y}) + \sum_{k_x}|k_x|^{-\alpha}\left|\frac{2\pi}{L_y}\right|^{-(\beta+1)}\cos(k_x x + \phi_y) \quad (2)$$

$$\delta B_z = \sum_{k_x}\sum_{k_y}\frac{|k_x|^{-\alpha}|k_y|^{-\beta}}{(k_x + k_y)}\cos(k_x x + k_y y + \phi_z), \quad (3)$$

where L_x and L_y are the box lengths, $k_x = 2\pi m/L_x$, $k_y = 2\pi n/L_y$, m and n are integers which usually range from -3 to 3, and $\phi_{x,y}$, ϕ_x, ϕ_y, ϕ_z are random angles. Note that the choice of δB_z is arbitrary and is made in such a way that its amplitude is of the order of the amplitudes of δB_x and δB_y. We have run several simulations with different values for the slopes α and β of the spectra and the results seem not to be significantly affected by those parameters, For simplicity, we will show the results when $\alpha = \beta = 0$.

As a further check on the soundness of the results, we have also initialized some simulations with a spectrum of waves with an Alfvènic velocity perturbation imposed, and the results are qualitatively similar for the length and timescales investigated here.

3. RESULTS

3.1. Turbulent Cascade

The first results that we show are for benchmark cases, where we have initialized the perturbation ($\delta B/B_0 \sim 1$) with a single wavenumber and not with a spectrum of waves. Figure 2 shows the developed spectrum of magnetic fluctuations $\delta B/B_0$ in wavenumber space at the end of the simulation. The only mode initially perturbed was the mode $m = 1, n = 3$, which is indicated with an arrow. The result indicates that the harmonics of the initial mode get predominantly excited according to a three-wave resonant interaction ($k = k_1 + k_2$). Clearly one cannot speak of turbulent cascade in this case, but the purpose of this simulation is to check whether the code is able to treat in a consistent and satisfactory manner injections of energy at small scales. An issue with PIC codes is indeed the unavoidable presence of noise at small scales due to the discreteness of computational particles. This noise could result in the spurious effect of an inverse cascade of energy from large wavenumbers which is completely numerically generated. One can see that this effect is not important in Figure 2, where the modes at large k that get excited are only the higher harmonics of the initial mode. The price to pay in order to avoid spurious effects at small scales is the use of an unusually large number of particles (6400 particles per cell).

A confirmation of the fact that three-wave resonant interactions are well described in the code is shown in Figure 3. In this case we have excited, along with the mode $m = 1, n = 3$, its counter-propagating mode $m = -1, n = 3$. The modes initially excited are circled. The resulting distribution of energy satisfies again the relation $k = k_1 + k_2$, giving rise to that checkerboard plot.

As we have said, these results should only be considered as benchmark runs. However, from Figures 2 and 3 it is already clear that the treatment of small amplitudes fluctuations at large k as linear modes poses some problems when the system

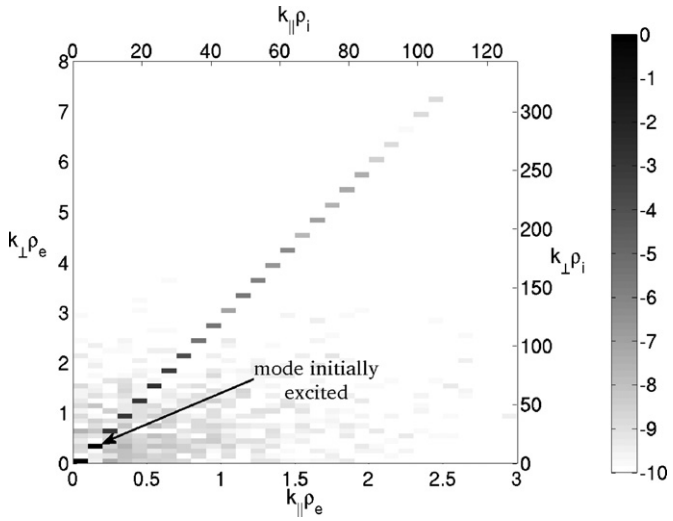

Figure 2. Spectrum of magnetic fluctuations $\delta B/B_0$ in wavenumber space in logarithmic scale. The mode initially excited $m = 1, n = 3$ is indicated with an arrow.

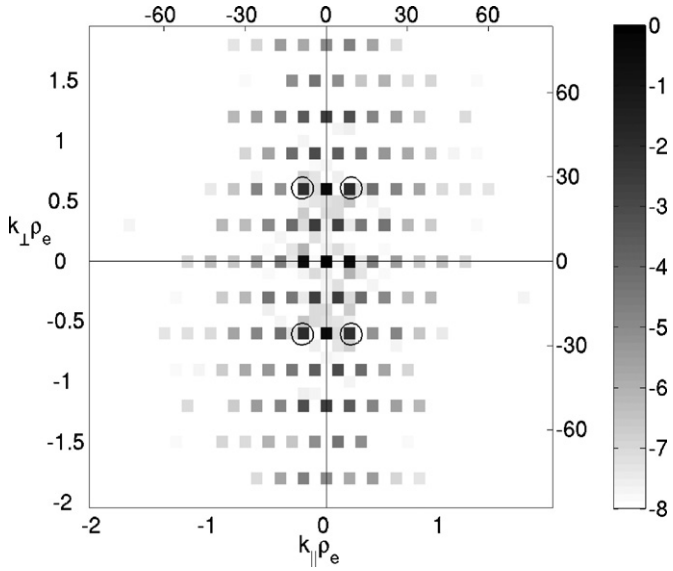

Figure 3. Spectrum of magnetic fluctuations $\delta B/B_0$ in wavenumber space in logarithmic scale. The modes initially excited $m = 1, n = 3$, and $m = -1$, $n = 3$ are circled.

allows the presence of finite amplitude perturbations at small k. This is because nonlinear interactions that couple small and large k modes could always take place, resulting in a continuous injection of energy at small scales. Hence, in order to characterize the dissipation range solely through some linear damping mechanism, one needs to find out at what scale the nonlinear coupling becomes completely ineffective. In other words, the fact that the amplitude of fluctuations is small at some scales does not alone justify the validity of linear theory in the solar wind. Another requisite is that those scales should not take part in any nonlinear coupling with larger scales. We now show and comment on the results of a run where a flat spectrum of modes has been excited, accordingly to Equations (1)–(3). The range of modes excited is (0, 3) in both wavenumbers m and n. As we said, we have tried different slopes for the initial spectrum, but we will comment on one run only, as the results were very similar.

Figures 4 and 5 show the spectra of $|\delta B|^2/|B_0|^2$ in parallel and perpendicular directions (i.e., integrated along the other

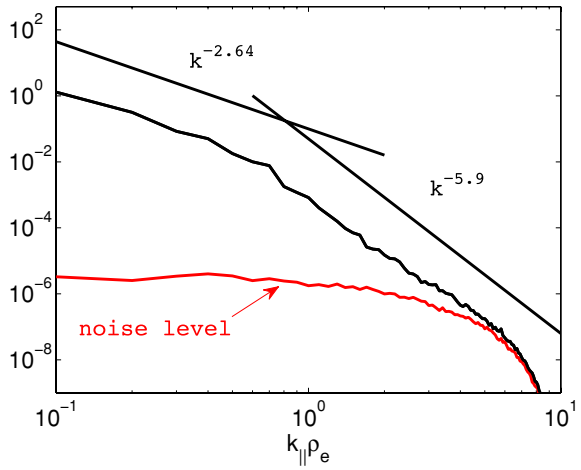

Figure 4. Spectrum of magnetic fluctuations $|\delta B|^2/|B_0|^2$ in the parallel direction $k\rho_{e\parallel}$. The noise level curve is in red. The power-law best fits are superimposed.
(A color version of this figure is available in the online journal.)

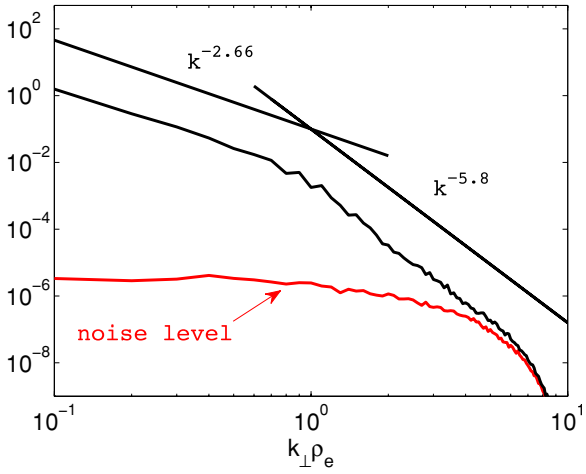

Figure 5. Spectrum of magnetic fluctuations $|\delta B|^2/|B_0|^2$ in the perpendicular direction $k\rho_{e\perp}$. The noise level curve is in red. The power-law best fits are superimposed.
(A color version of this figure is available in the online journal.)

direction), respectively. The red curve indicates the noise level, which is the level of fluctuations generated by particle noise, when no initial perturbation is imposed in the equilibrium. As it is clear, results above $k\rho_e \sim 7$ are not reliable, because the curves approach the noise level. Moreover, in order to be far enough from the noise level, and allow the cascade to proceed as much as possible, we initialize the perturbation with a relatively large amplitude ($\delta B/B_0 \sim 3$), at $k\rho_e = 0.1$. This is not completely consistent with solar wind observations, but it does not affect the purpose of this study, because the amplitude of fluctuations above $k\rho_e = 1$ is small enough, in principle, to justify the comparison with linear theory which is presented in the next section. The spectra presented in Figures 4 and 5 are fully converged. The cascade proceeds very quickly and reaches a stationary profile after about $T\Omega_e \sim 30$. Of course, in reality, there may be evolution on timescales longer and length scales larger than those simulated. This could only be investigated with considerably larger and longer simulations.

Two interesting features emerge from Figures 4 and 5. First, the spectrum develops a well-defined power law that steepens at about the inverse electron gyroradius. The plots

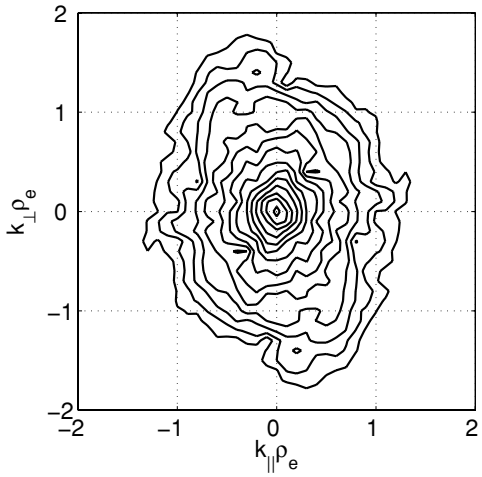

Figure 6. Contour plot of the spectrum of magnetic fluctuations $|\delta B|^2/|B_0|^2$ in parallel and perpendicular directions. The contours are for values of $10^{-15}, 10^{-14}, \ldots, 10^{0}$.

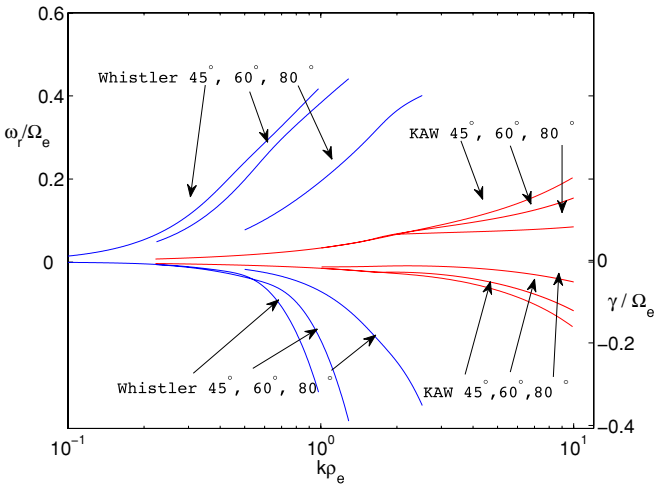

Figure 7. Dispersion curves for KAWs and whistler modes for different angles of propagation: $\theta = 45^\circ, 60^\circ$, and 80°. Frequencies are normalized on the electron cyclotron frequency Ω_e (ω_r is the real frequency and γ is the damping rate). (A color version of this figure is available in the online journal.)

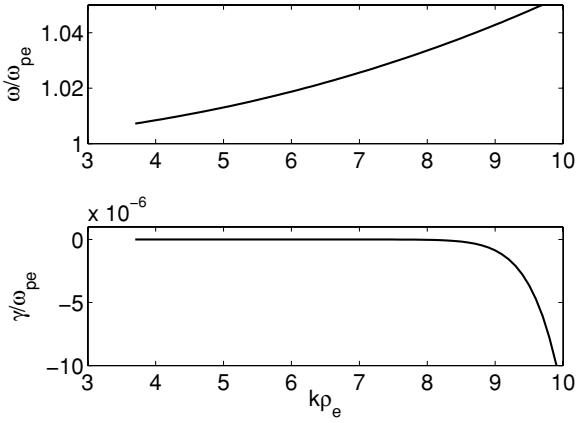

Figure 8. Frequency (top) and damping rate (bottom) for the Langmuir mode at $\theta = 80^\circ$, normalized on the electron plasma frequency ω_{pe}.

show that the least-squared fit with a power-law function yields exponents which are consistent with solar wind observations (in particular $|\delta B/B_0|^2 \sim k^{-2.6}$ between the ion and electron inverse gyroradii, although this feature might be coincidental due to the two-dimensional character of the simulations). Second, the nonlinear cascade proceeds far into the electrons scales, until it reaches the noise level. There is no sign of an exponential roll over or the emergence of linear dissipation mechanisms, even when the level of $\delta B/B_0$ is as low as 10^{-2}, which usually considered small enough for applying linear theory.

The nonlinear cascade proceeds as it is expected in magnetized plasma (Chen et al. 2010). It develops the well-known power anisotropy, which means that most of the energy resides, at the end of the simulation, in oblique or quasi-perpendicular modes. This is visible in Figure 6, where we show the spectrum of magnetic perturbations as a contour plot in wavevector space.

3.2. Comparison with Linear Theory

In previous works, it has been argued that the dynamics of the dissipation at small scales can be described by linear mechanisms, since the amplitude of fluctuations become so small that nonlinear effects can be neglected. It is also argued that a purely linear damping mechanism will result in an exponential roll over of the spectrum of turbulent fluctuations. In this section, we attempt to interpret the simulation results at the light of Vlasov linear theory. We have used a Vlasov solver to identify linear modes in the range of wavevectors of interest for this study. We anticipate that, at these scales, it becomes very difficult to follow the numerical solution of the dispersion relation for one single mode, as many branches of the solutions overlap. We show in Figures 7 and 8, the dispersion relations for whistler modes, KAWs, and Langmuir waves, for different angles of propagation ($\theta = 45^\circ, 60^\circ$, and 80°). We focus attention on oblique modes, since we know that the cascade tends to develop the aforementioned anisotropy. We point out that what we call Langmuir waves are the generalization of electrostatic Langmuir modes in presence of the magnetic field, studied in Willes & Cairns (2000). They are lightly damped high-frequency oscillations, which are not usually taken in account in this regime.

The same dispersion curves for the damping rate only of KAWs and whistler modes are plotted in log–log scale in Figure 9. Li et al. (2001) have proposed an empirical fit for the damping rate γ of KAWs of the form

$$\gamma = -m_1 k^{m_2} e^{-\left(\frac{m_3}{k}\right)^2}, \quad (4)$$

where m_1, m_2, and m_3 are positive fitting parameters. They have also argued, on the basis of a simplified model, which treats the nonlinear cascade as an isotropic diffusion process in wavenumber space, that in order to recover a power law for the spectrum of magnetic fluctuations, the damping rate should be itself a power law as a function of k. What is interesting, in Figure 9, is that at this scale the damping rate seems to follow precisely a power law in k. The form of Equation (4) could still be valid, but the exponential factor becomes essentially very close to 1, as k becomes very large.

Another interesting feature of Figure 9, which has not been previously commented on elsewhere, is that the damping rate of KAWs and whistler modes undergoes a smooth transition from a certain power law to another. In principle, one could argue that the dispersion curves of Figures 7 and 9 might account for the results of Figures 4 and 5, i.e., for the cascade of the power spectrum and its steepening, since the properties of the linear

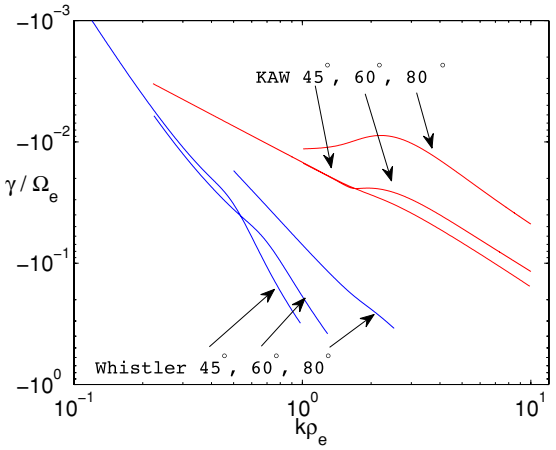

Figure 9. Damping rates for KAWs and whistler modes for different angles of propagation: $\theta = 45°$, 60°, and80°, in log–log scale, normalized on the electron cyclotron frequency Ω_e.

(A color version of this figure is available in the online journal.)

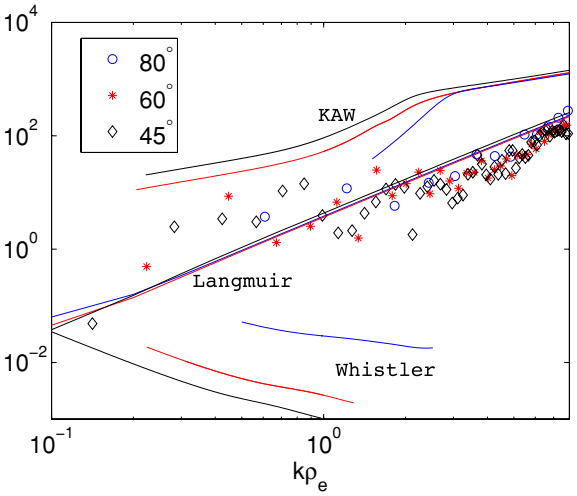

Figure 10. Electron compressibility $|\delta n_e|/|\delta B|$. The symbols are the results of simulations (circle for $\theta = 80°$, star for $\theta = 60°$, and diamond for $\theta = 45°$). Solid lines are the predictions from linear Vlasov theory for KAWs, whistler modes, and Langmuir waves (in blue for $\theta = 80°$, red for $\theta = 60°$, and black for $\theta = 45°$).

(A color version of this figure is available in the online journal.)

waves, at this scale, seem to be favorable for the support of a power-law solution for the fluctuations. However, if this is the case, we still need a firm characterization of the fluctuations in terms of linear waves.

Following Gary & Smith (2009), we now try to characterize the linear waves by their electron compressibility $\delta n_e/\delta B$. We prefer to use the electron compressibility rather than the magnetic compressibility, because the former gives a better signature of the difference between KAWs and whistler modes. Indeed, for KAWs the electron compressibility grows as a function of k, while it decreases for whistlers. In Figure 10, we show the values of the electron compressibility calculated from the simulation for different angles of propagation (diamonds for $\theta = 45°$, stars for $\theta = 60°$, and circles for $\theta = 80°$). The solid lines indicate the value predicted for KAWs, whistlers and Langmuir modes. The simulation results clearly indicate a trend of increasing values for larger values of $k\rho_e$, which suggests a certain degree of Alfvènicity of the fluctuations. However, none of the linear modes taken into consideration are in good agreement with the

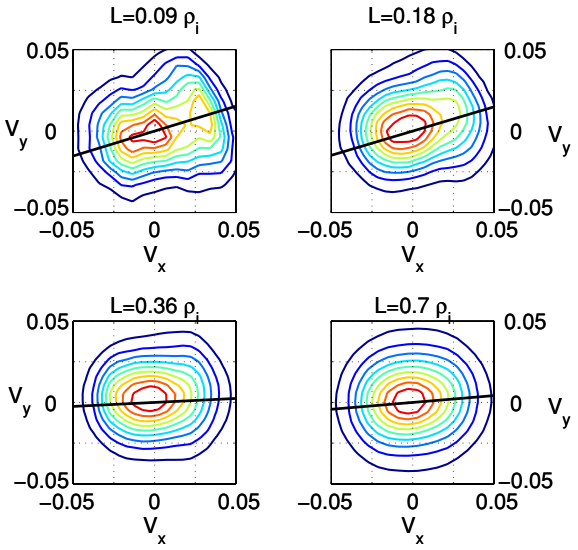

Figure 11. Electron distribution functions in the (x, y)-plane, collected in four nested boxes of increasing size L. The solid line shows the direction of the mean magnetic field within each box. Velocities are normalized to the speed of light.

(A color version of this figure is available in the online journal.)

simulation result. The fluctuations are probably a mixture of different modes. Interestingly, the Langmuir mode seem to be the one whose electron compressibility is closest to the simulations results. This might be related to the high level of initial fluctuations.

3.3. Particle Heating

The energy at the beginning of the simulations is partitioned equally between the magnetic field and the particles, and electrons and ions have the same kinetic energy. The simulation conserves more than 95% of the total energy, and at the end of the run there is a 5% increment of the total kinetic energy, at the expense of magnetic energy. The increase in electric energy is negligible. The heating is directed mainly to electrons, such that at the end of the simulation they are 20% hotter than the protons. This is however not surprising, given the time and length scales of the simulations.

Electrons are heated predominantly in the parallel direction (with respect to the magnetic field). The value of temperature anisotropy is not constant over the whole computational domain, but depends on the spatial position, and $T_\parallel/T_\perp$ ranges from 0.98 to 4.9. This suggests that the heating is connected with the formation of magnetic topological structures. An interesting feature that emerges by examining the electron distribution function is the presence of non-thermal features. However, the deviation from a bi-Maxwellian distribution is more accentuated when the particles and the mean magnetic field are considered in a small portion of the box. We show in Figure 11 the electron distribution function in the (x, y)-plane for four different nested boxes. Velocities are normalized to the speed of light. The solid line indicates the direction of the mean magnetic field within each box, and L is the length of the boxes, in ion gyroradius units. It turns out that as the magnetic field and the particles are averaged over larger and larger boxes, the distribution function tends to become more and more bi-Maxwellian and any non-thermal feature is lost. A similar result holds in the (x, z)-plane, while the distributions in the direction orthogonal to the mean magnetic field remain roughly gyrotropic. This result has important implications for satellite observations. Indeed, it

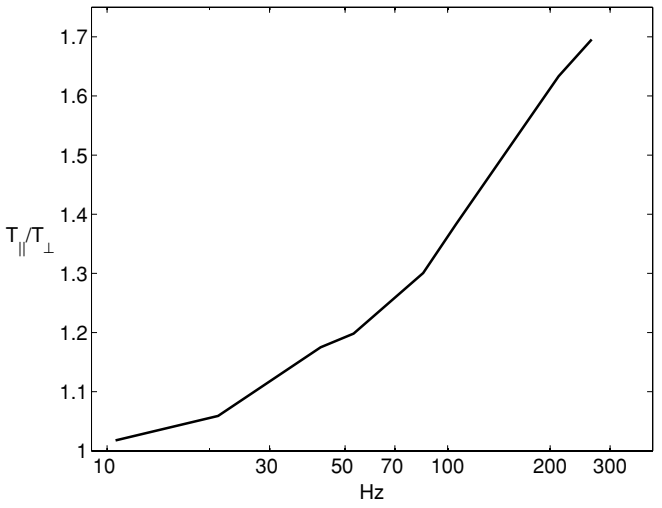

Figure 12. Electron anisotropy $T_\parallel/T_\perp$ vs. the frequency at which data are collected in Hz.

suggests that the time window over which the particles and the magnetic field are averaged affects the distribution functions and therefore the anisotropy measured. By assuming a steady wind flowing at 250 km s^{-1}, one can transform the box lengths into frequencies at which data are collected, and estimate what is the level of anisotropy measured at different frequencies. The upper bound of such anisotropies are shown, for electrons, in Figure 12. Given the small length of the computational box used in this study, the range of frequencies plotted in Figure 12 is relatively high. However, future missions and instruments may be able to collect data at such frequencies, and therefore will be able to verify this prediction.

4. CONCLUSION

We have performed two-dimensional fully kinetic PIC simulations of decaying magnetic fluctuations at electron scales. The scope of this work is to address some open questions regarding the dissipation of turbulent fluctuations at small scales and the plausibility of treating such fluctuations in the framework of linear theory.

We have shown the results of the first simulations that use realistic parameters in a fairly large computational domain that extends to electron scales. This represents an improvement in the context of the previous two-dimensional simulations.

The results of our simulations suggest that a turbulent cascade in the form of a power law could proceed very far below the electron gyroradius. It is interesting that at such scales the respective damping rates for both KAWs and whistler modes are power laws as a function of k. In principle, this would suggest that purely linear mechanisms could be responsible for a power-law spectrum of fluctuations, such as the one observed in satellite data, and obtained in the PIC simulations. However, we have shown that neither KAWs nor whistler modes have an electron compressibility that is in agreement with simulations results.

Our interpretation is that many different modes should be taken in account at this scale, including Langmuir waves and possibly other more heavily damped modes. Unfortunately, the level of excitation of each mode depends on nonlinear mechanisms active at larger scale. Therefore, we doubt that the dissipation process can be understood and described solely within a linear description. However, the puzzling steepening of the power spectrum might be caused by changes of the linear properties of the waves, as the ones reported in Figure 9. Concerning the heating of the particles, we have observed a preferential heating of electrons along the parallel direction (the same happens, in smaller measure, to protons, but the size of the box does not really allow us to draw any informative conclusions on protons). It has also emerged that non-thermal features in the electron distribution function appear when the box over which quantities are averaged is not too large (i.e., smaller than 0.2–0.3 ρ_i). On the basis of this result, we have made a prediction of the upper bound value of electron anisotropy related to the frequency at which data are collected, which can be verified by future measurements.

A last comment on the computational aspects of this work is due. The results presented in this paper have been obtained essentially thanks to the use of a semi-implicit code. This has allowed us to use a computational box that comprehends scales as small as $k\rho_e = 10$ and as large as $k\rho_i \sim 4$. However, in order to keep a low level of noise we had to use a large number of particles per cell. At present, this excludes the possibility of extending the box to fully include ion scales and constrains the geometry to be two dimensional. We used a two-dimensional computational spatial domain which contains the background magnetic field; the particle velocity space is three dimensional. This restricts the available k-space for fluctuations to a $(k_\parallel, k_\perp)$ plane, with the consequence, particularly, of restricting, but not entirely eliminating, the interaction of modes with k strictly perpendicular to the magnetic field. However, the use of this particular choice of simulation plane retains fluctuations with a $k_\parallel$ component and the possibility of particle parallel scattering and heating, and is thus a more realistic choice than having the background magnetic field strictly perpendicular to the simulation plane. For these reasons, we believe the two-dimensional results we have presented are qualitatively robust, but, of course, they will only be confirmed by fully three-dimensional simulations. Of course, this is now at the edge of computational feasibility, but a possibility worth investigating in the future is the performance of an implicit δf-PIC simulation, so that the number of particles needed could be reduced.

This work was supported by STFC grant ST/H002731/1.

REFERENCES

Alexandrova, O., Saur, J., Lacombe, C., Mangeney, A., Mitchell, J., Schwartz, S. J., & Robert, P. 2009, Phys. Rev. Lett., 103, 165003
Camporeale, E., Passot, T., & Burgess, D. 2010, ApJ, 715, 260
Chen, C. H. K., Horbury, T. S., Schekochihin, A. A., Wicks, R. T., Alexandrova, O., & Mitchell, J. 2010, Phys. Rev. Lett., 104, 255002
Coleman, P. J. 1968, ApJ, 153, 371
Galtier, S., & Buchlin, E. 2007, ApJ, 656, 560
Gary, S. P., Saito, S., & Li, H. 2008, Geophys. Res. Lett., 35, 2104
Gary, S. P., & Smith, C. W. 2009, J. Geophys. Res., 114, 12105
Howes, G. G., Cowley, S. C., Dorland, W., Hammett, G. W., Quataert, E., & Schekochihin, A. A. 2008a, J. Geophys. Res., 113, A05103
Howes, G. G., Dorland, W., Cowley, S. C., Hammett, G. W., Quataert, E., Schekochihin, A. A., & Tatsuno, T. 2008b, Phys. Rev. Lett., 100, 065004
Jiang, Y. W., Liu, S., & Petrosian, V. 2009, ApJ, 698, 163
Leamon, R. J., Matthaeus, W. H., Smith, C. W., & Wong, H. K. 1998a, ApJ, 507, L181
Leamon, R. J., Smith, C. W., Ness, N. F., Matthaeus, W. H., & Wong, H. K. 1998b, J. Geophys. Res., 103, 4775
Leamon, R. J., Smith, C. W., Ness, N. F., & Wong, H. K. 1999, J. Geophys. Res., 104, 22331
Li, H., Gary, S. P., & Stawicki, O. 2001, Geophys. Res. Lett., 28, 1347
Markidis, S., Camporeale, E., Burgess, D., Rizwan-Uddin,, & Lapenta, G. 2009, in ASP Conf. Ser. 406, Numerical Modeling of Space Plasma Flows:

ASTRONUM-2008, ed. N. V. Pogorelov et al. (San Francisco, CA: ASP), 237
Markovskii, S. A., Vasquez, B. J., & Chandran, B. D. G. 2010, ApJ, 709, 1003
Matthaeus, W. H., Weygand, J. M., Chuychai, P., Dasso, S., Smith, C. W., & Kivelson, M. G. 2008, ApJ, 678, L141
Parashar, T. N., Shay, M. A., Cassak, P. A., & Matthaeus, W. H. 2009, Phys. Plasmas, 16, 032310
Podesta, J. J., Borovsky, J. E., & Gary, S. P. 2010, ApJ, 712, 685
Sahraoui, F., Goldstein, M. L., Belmont, G., Canu, P., & Rezeau, L. 2010, Phys. Rev. Lett., 105, 131101
Sahraoui, F., Goldstein, M. L., Robert, P., & Khotyaintsev, Y. V. 2009, Phys. Rev. Lett., 102, 231102
Saito, S., Gary, S. P., Li, H., & Narita, Y. 2008, Phys. Plasmas, 15, 102305
Smith, C. W., Hamilton, K., Vasquez, B. J., & Leamon, R. J. 2006, ApJ, 645, L85
Stawicki, O., Gary, S. P., & Li, H. 2001, J. Geophys. Res., 106, 8273
Svidzinski, V. A., Li, H., Rose, H. A., Albright, B. J., & Bowers, K. J. 2009, Phys. Plasmas, 16, 122310
Valentini, F., Califano, F., & Veltri, P. 2010, Phys. Rev. Lett., 104, 205002
Willes, A. J., & Cairns, I. H. 2000, Phys. Plasmas, 7, 3167

The Astrophysical Journal, 735:67 (2pp), 2011 July 1 doi:10.1088/0004-637X/735/1/67
© 2011. The American Astronomical Society. All rights reserved. Printed in the U.S.A.

ERRATUM: "THE DISSIPATION OF SOLAR WIND TURBULENT FLUCTUATIONS AT ELECTRON SCALES" (2011, ApJ, 730, 114)

Enrico Camporeale[1] and David Burgess[2]
[1] T-5 Applied Mathematics and Plasma Physics, Los Alamos National Laboratory, Los Alamos, NM 87545, USA
[2] School of Mathematical Sciences, Queen Mary University of London, Mile End Road, London E1 4NS, UK
Received 2011 April 29; published 2011 June 16

Online-only material: color figures

In the published paper, we misinterpreted a solution of the hot plasma dispersion relation. What we identified as a kinetic Alfv́en wave is instead a mode that can be identified as the ion-acoustic wave, when tracked to parallel propagation. Although it is purely electrostatic when parallel propagating, it becomes more and more electromagnetic when it propagates at large angles. For the regime studied in the paper, this mode has to be taken into account, since it is one of the least damped modes of the linear Vlasov equation. However, the exact role of the ion-acoustic mode for the damping of turbulent fluctuations will require further investigation. We note that in this regime the kinetic Alfv́en wave is more heavily damped. The misinterpretation of that mode does not alter the results and the conclusions of the paper. For clarity we present some of the figures derived from the linear dispersion relation shown in the published paper, with corrected notations and captions (Figures 1–3).

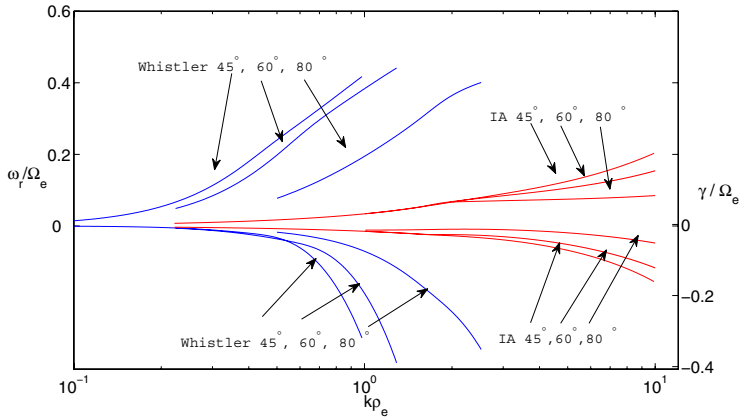

Figure 1. Dispersion curves for ion-acoustic and whistler for different angles of propagation: $\theta = 45^\circ, 60^\circ,$ and 80°. Frequencies are normalized on the electron cyclotron frequency Ω_e.

(A color version of this figure is available in the online journal.)

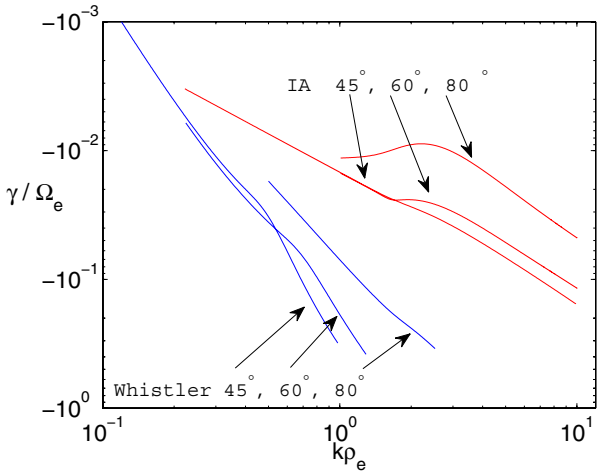

Figure 2. Damping rates for ion-acoustic and whistler for different angles of propagation: $\theta = 45^\circ, 60^\circ,$ and 80°, in log–log scale, normalized on the electron cyclotron frequency Ω_e.

(A color version of this figure is available in the online journal.)

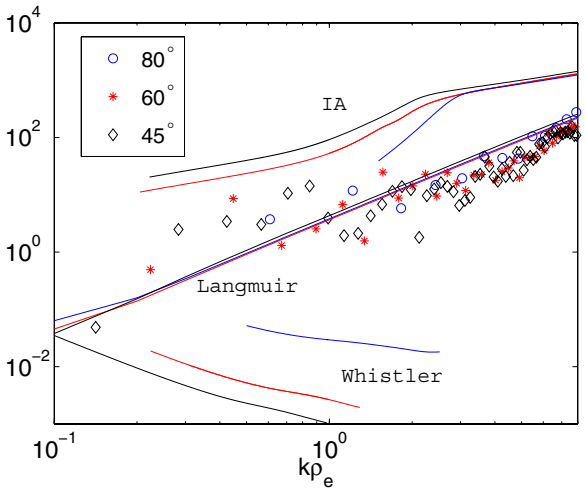

Figure 3. Electron compressibility $|\delta n_e|/|\delta B|$. The symbols are the results of simulations (circle for $\theta = 80°$, star for $\theta = 60°$, and diamond for $\theta = 45°$). Solid lines are the predictions from linear Vlasov theory for ion-acoustic, whistler, and Langmuir waves (in blue for $\theta = 80°$, red for $\theta = 60°$, and black for $\theta = 45°$).
(A color version of this figure is available in the online journal.)

We thank S. Peter Gary who pointed out the misinterpretation in the paper, and for helping to clarify the true nature of that linear mode.